PHY378 Final Report: Phonon Physics in SuperCDMS HV Detector

Stephanie Cui, Department of Physics, University of Toronto
Supervised by Prof. Pekka Sinervo

December 2024

1 Abstract

The study investigates the phonon physics in the Super Cryogenic Dark Matter Search (SuperCDMS) High Voltage (HV) detector. In particular, we analyzed the effect of surface anharmonic phonon down-conversion on the phonon energy collection efficiency and phonon energy distribution among detector channels. By generating simulation samples at the Detector Monte Carlo (DMC) stage, we compared these features in the simulated samples and real data sets taken at the Cryogenic Underground TEst (CUTE) facility with simulated samples. We discovered that simulating surface down-conversion not only lowers the mean phonon energy collection efficiency from unrealistic values but also resolves the discrepancy previously found between simulated and experimental data in the energy absorption of the two outer ring channels (A and B). Using a down-conversion rate of 8.3×10^{18} Hz, the mean energy collection efficiency decreased by approximately 45%, and the collection efficiencies exhibited a clearer dependence on radial position. The percentages of energy collected by the A and B channels were both reduced to values that align with real data.

2 Experimental Background

The Super Cryogenic Dark Matter Search (SuperCDMS) is a dark matter direct detection experiment at SNOLAB. It utilizes phonon and charge sensors to detect the interaction of Weakly Interacting Massive Particles (WIMPs) with detectors made of Germanium and Silicon crystals. The SuperCDMS High Voltage (HV) detector aims to detect the energy deposition of WIMPs through heat in the form of phonons, which are vibrational quantum states within the crystal lattice. When a WIMP interacts with the detector crystal, recoil or primary phonons are generated at the location of the energy deposition and propagate isotropically. The phonon production is then amplified by the Neganov-Trofimov-Luke (NTL) effect due to the electric field created by an applied voltage [2]. The electron-hole pairs produced from the energy deposition also accelerate due to the electric field. The total phonon energy generated is the energy of the recoil phonons and the NTL phonons:

$$E_{\mathrm{ph}} = E_{\mathrm{recoil}} + E_{\mathrm{NTL}} \tag{1}$$

The HV detector is cylindrical in shape, with its upper and lower surfaces covered in transition edge sensors (TESs), which are tungsten strips with fan-shaped Aluminum traps [2]. Phonons that reach the transition edge sensors can (with sufficient energy) break the cooper pairs within the Al fins. The quasi-particles produced then heat up the tungsten that gets transferred into electrical signal.

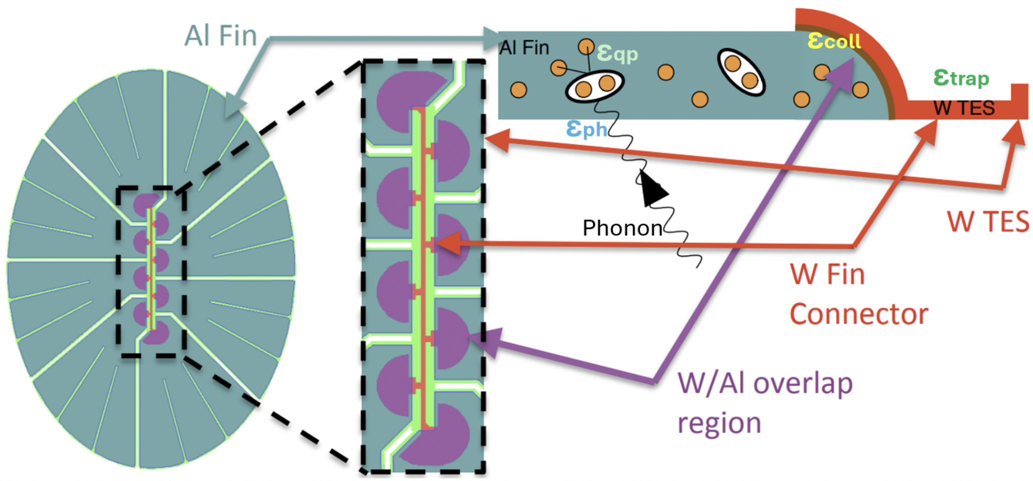

Figure 1: Diagrammatic representation of the tungsten Transition Edge Sensors and the phonon-trapping Aluminum fins [10].

The two sides of the detector are each divided into six phonon sensing channels, with a total of 12 channels. The channels were designed to have approximately equal area (see Figure 2).

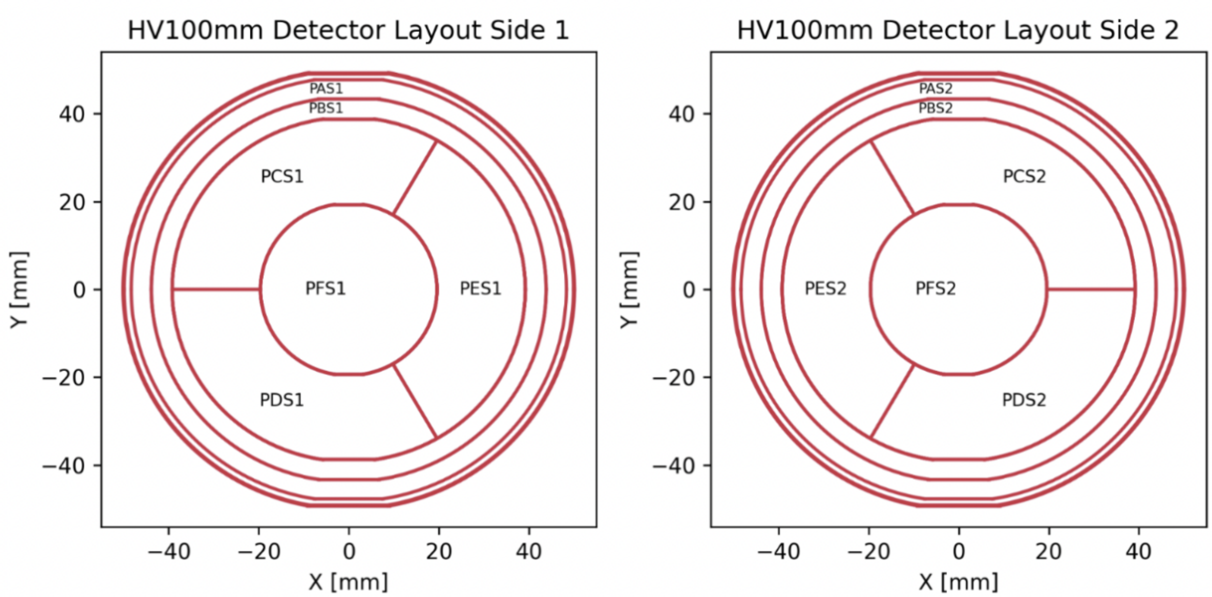

Figure 2: Two sides of HV100mm Detector Layout. The channels are labeled by a letter and their corresponding side (1 or 2). Note the two outer ring channels (A and B) and the inner core channel (F) are directly above each other, whereas the wedge-shaped channels (C, D, and E) are rotated and/or reflected away from each other.

3 Phonon Transport, Scattering, and Down-conversion

Phonons can be classified into two vibrational modes: acoustic (where two atoms in the primitive cell move in phase) and optical (where two atoms in the primitive cell move out-of-phase) [6]. Since optical phonons rapidly down-convert to more long-lived acoustic phonons in millikelvin environments, only acoustic phonons are modeled in our simulation [3]. Furthermore, these vibrational states have three distinct polarizations: slow transverse (ST), fast transverse (FT), and longitudinal (L). The speed and polarization mode occurrence can be determined for a diffusive phonon, which produces an estimated average speed of 3550 m/s [6].

Phonon propagation within the crystal can be described by the three-dimensional wave equation:

$$\rho\omega^2\epsilon_\mu = \sum_\tau \left(\sum_{\sigma\nu} c_{\mu\sigma\nu\tau} q_\sigma q_\nu\right)\epsilon_\tau, \tag{2.26}$$

where ρ is the mass density of the crystal, ω is the phonon angular frequency, ϵ_μ is a component of its polarization vector $\boldsymbol{\epsilon}$, $c_{\mu\sigma\nu\tau}$ is the elastic tensor, and q_σ is a component of its wave vector $\mathbf{q}$ [5].

The direction and velocity of phonon propagation is given by the group velocity:

$$\mathbf{v}_\mathrm{g} = \nabla_\mathbf{q}\omega(\mathbf{q}) \tag{2.27}$$

which may not be parallel to the phonon momentum $\hbar\mathbf{q}$ [**?**]. Instead, phonons are focused into directions that correspond to the highest density of eigenvectors [3]. This gives rise to the anisotropic transport of phonons.

In addition, phonons interact with isotopic substitution sites in the lattice and elastically scatter. This process, known as isotopic scattering, randomizes the phonon momentum vector and the polarization state [3]. The rate at which it occurs is given by

$$\Gamma_\mathrm{scatter} = B\nu^4 \tag{2}$$

where the coefficient $B = 3.67\times10^{-41}$ s^3 is given in literature [**?**].

Furthermore, phonons lose energy within the detector crystal through the process of anharmonic down-conversion, where a high energy phonon splits into two lower energy phonons. Energy is conserved (so the energy of the daughter phonons sum to the original phonon's energy), but momentum is exchanged with the crystal lattice [3]. In the isotropic model, transverse phonons do not undergo this splitting due to energy and momentum conservation.

Initially, the energy deposition E_ph is high enough such that the phonons move in a random walk, as seen in the purple track in Figure 3, where the 40 meV phonon scatters frequently in various directions. Only when the phonon energy is lower than the ballistic threshold, $E_\mathrm{ballistic}\approx 250$ GHz can it travel ballistically and reach the detector surface. Indeed, the blue and green tracks display lower-energy phonons traveling quasi-ballistically after down-conversion. Phonons with an energy greater than $2\Delta E_\mathrm{Al\ gap}\approx 340\times10^{-6}$ eV, where ΔE_gap is the subgap energy of the semiconductor, can break an aluminum cooper pair. This breaking of cooper pair allows for the collection of phonons in the Al fins on the detector surface. It is notable that interactions with the Al fins will dominate further phonon down-conversion processes, so we expect a large amount of phonons to be absorbed rather than fall below the $2\Delta E_\mathrm{Al\ gap}$ threshold and undergo full thermalization.

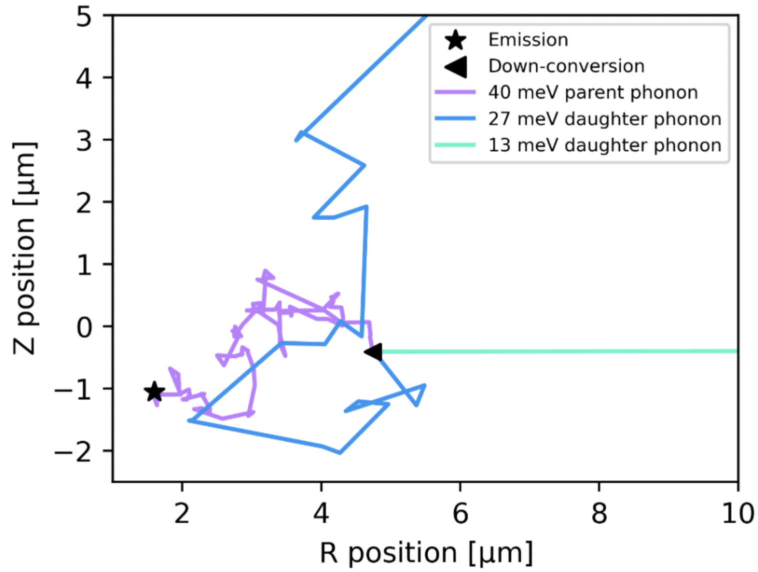

Figure 3: Z position vs R position plot with phonon tracks drawn in different colors [11].

The down-conversion process within the bulk of the detector is well-known and occurs at the rate of

$$\Gamma_{\text{anh}} = A\nu^5$$

anharmonic down-conversion events per unit time, where ν is given by the phonon energy E_{ph} divided by Planck's constant h. The coefficient, A, can be calculated from experimentally measured constants that are substrate-dependent [?].

Note that anharmonic down-conversion occurs less frequently than isotopic scattering for a 40 meV phonon, evident in Figure 3. We can verify by calculating its phonon frequency:

$$\nu = \frac{40 \times 10^{-3}\ \text{eV}}{4.13 \times 10^{-15}\ \text{eV}} \approx 10 \times 10^{12}\ \text{Hz} \tag{3}$$

and its scattering and down-conversion rates:

$$\Gamma_{\text{anh}} = A\nu^5 \approx 1.6456 \times 10^{-54}\ \text{s}^4 \times 10^{65}\ \text{s}^{-5} = 1.6456 \times 10^{11}\ \text{Hz}$$
$$\Gamma_{\text{scatter}} = B\nu^4 \approx 3.67 \times 10^{-41}\text{s}^3 \times 10^{52}\ \text{s}^{-4} = 3.67 \times 10^{11}\ \text{Hz}$$

which implies that isotopic scattering occurs approximately twice as often as anharmonic down-conversion.

Notably, phonon down-conversion is less well understood at detector surfaces, where phonons can down-convert and/or reflect specularly or diffusely [4]. The probabilities of each of these processes are not known. Currently, the reflection at the detector surfaces is modeled to be a hundred percent diffuse. The implementation of down-conversion will be discussed in length in the next section.

4 Current Implementation of Anharmonic Down-conversion

SuperCDMS employs the Geant4 Condensed Matter Physics (G4CMP) package to simulate phonon and charge transport within the detector crystal [3]. Anharmonic down-conversion is simulated alongside isotopic scattering (when a phonon interacts with an isotopic substitution site in the lattice) as the two phonon scattering processes that affect phonon transport. Since the transverse phonons do not undergo down-conversion under the isotropic model, the two types of longitudinal down-conversion process modeled are:

$$\mathrm{L} \rightarrow \mathrm{L'} + \mathrm{T} \quad \text{and} \quad \mathrm{L} \rightarrow \mathrm{T} + \mathrm{T} \tag{4}$$

where $\mathrm{L} \rightarrow \mathrm{T} + \mathrm{T}$ is the dominant type, which is set to be 74% of total down-conversions [?]. It is notable that this dominant process produces transverse phonons that can no longer down-convert in our simulation.

As mentioned in Section 3, the coefficient (A) that scales the bulk down-conversion rate with the phonon frequency can be estimated for different substrates. When using Ge higher order elastic constants measured at 3K, the coefficient was found to be 1.62×10^{-54} s^4 [7]. Yet, the elastic constants measured at 300K (with the same apparatus and methods) were in conflict with results of other experiments with higher sensitivity [?]. Using the high temperature constants, A is estimated to be 6.43×10^{-55} s^4, which is lower than the 3K value by a factor of 3. The coefficient currently implemented in G4CMP is 1.6456×10^{-54} s^4 [?].

The default G4CMP configuration does not model surface anharmonic down-conversion. In order to set surface anharmonic down-conversion, one must include an additional macro command line:

```
CDMS/Zip/Set<Section><Process>Reflectivity <c0><c1>...<c5> <unit> <Cutoff>
```

`<Section>` can be set to `Side`, `Top`, `Bottom`, and/or `All`. `Side` refers to the bare detector sidewall, `Top` and `Bottom` refer to the top and bottom detector surfaces without TES coverage, and `All` refers to all the above surfaces combined. Note that the surface area of the top and bottom bare surfaces is quite small compared to that of the sidewall. Moreover, `<Process>` can be set to specular reflection, diffuse reflection, and/or anharmonic down-conversion. In this study, we only experiment with the effect of simulating surface down-conversion. The total of six coefficients correspond to those in the following power series expansion [4]:

$$\Gamma_{\mathrm{anh}}(\nu) = c_0 + c_1\nu + c_2\nu^2 + c_3\nu^3 + c_4\nu^4 + c_5\nu^5 \tag{5}$$

where ν is again the phonon frequency. In this study, we only adjust the coefficient of the highest order term, c_5, and set all other coefficients to 0, reducing the above expansion to Equation **??**.

`<Cutoff>` is the frequency above which anharmonic down-conversion does not occur. This is a computational threshold that is set to 0 for this study.

5 Diagnostics

The diagnostics used to evaluate the effect of surface anharmonic down-conversion are the phonon energy collection efficiency of the TESs and the energy distribution among the detector channels. In simulated samples, the phonon energy collected is output by the DMC. In real data, raw pulses are processed using the reconstruction software CDMSBats, which outputs pulse amplitudes that are proportional to the amount of energy collected [2].

The phonon energy collection efficiency represents the probability that a phonon produced is absorbed by an Al fin:

$$\epsilon_{\mathrm{ph}} = E_{\mathrm{absorbed}}/E_{\mathrm{ph}} \tag{6}$$

where E_{absorbed} is the energy collected by the TESs and E_{ph} is the total phonon energy from an energy deposition (sum of the recoil energy and the NTL energy [2]):

$$E_{\text{ph}} = E_{\text{recoil}} \left(1 + \frac{e\Delta V}{E_{\text{ionization}}}\right) \tag{7}$$

where $E_{\text{ionization}}$ is the energy required to ionize an electron in the detector crystal (2.96 eV for Germanium and 3.81 eV for silicon).

It is clear that simulating surface down-conversion will affect ϵ_{ph} since the number of phonons with energy more than $2\Delta E_{\text{gap}}$ is expected to decrease when phonons split into lower energies at the surfaces.

The distribution of phonon energy among detector channels is another useful diagnostic because of their radial position dependence. Due to the HV detector channel layout, events where a channel records the maximum phonon energy across one side are likely to have occurred with a radial position within the channel region. Indeed, the position dependence of the pulse amplitudes (and hence the phonon energies collected) was verified in the DMC (see [2]), and we expect the same position dependence to be present in real data.The DMC outputs the energy collected by every channel for each event, so we could sum up the energy collected by each channel across all events and divide by the total energy collected across all events to obtain the percentage of energy absorption by each channel.

6 Results and Discussions

6.1 Eliminating Phonons with Energy Below $2\Delta E_{\textbf{Al gap}}$

As mentioned in Section 3, phonons with energy below $2\Delta E_{\text{Al gap}}$ cannot break aluminum Cooper pairs and, therefore, cannot be detected by TESs. To improve computational efficiency in terms of time and memory, we eliminated (did not track) phonons with energy below this threshold during the simulation of 100 energy depositions using the command:

```
/g4cmp/minEPhonons 340e-6 eV
```

The phonon energy collection efficiencies for the 0V and 50V DMC samples were found to be around 100% and 88%, respectively. Although an estimate of experimental collection efficiency is lacking, these values are too high and reflect the many idealizations in the simulation.

Figure 4 shows that eliminating phonons below the Al conducting gap reduces the collection efficiency by approximately 11% for both the 0 V and 50 V samples. This result contradicts our initial assumption that the absence of low-energy phonons would not impact ϵ_{ph}. However, due to the way phonon absorption is modeled in the G4CMP, all phonons are eventually collected by the tungsten TESs. In the simulation, phonons that reach Al fins but have energies lower than $2\Delta E_{\text{Al gap}}$ are reflected diffusely back into the crystal. Moreover, there exists a sub-gap absorption parameter that defines the probability for low-energy phonons to be directly absorbed by the TESs [3]. Thus, only a small amount total phonon energy is lost. This modeling explains why we obtained unrealistically high collection efficiencies.

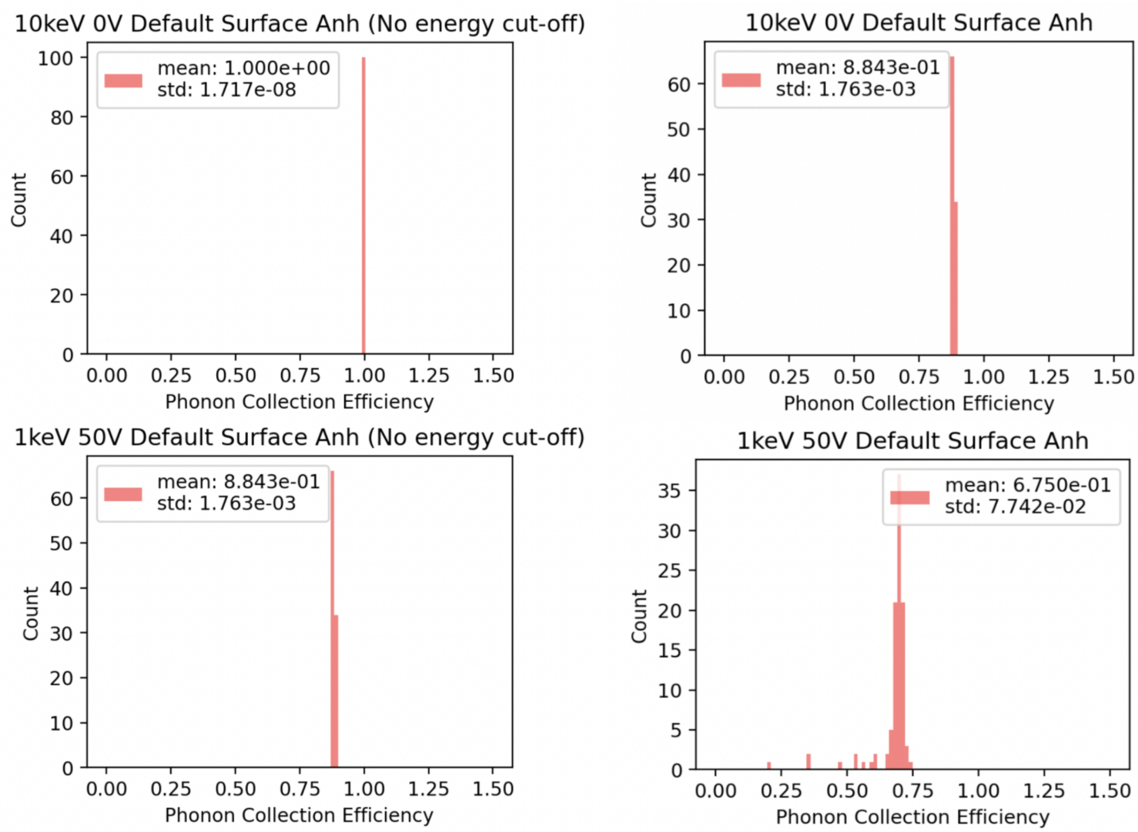

Figure 4: Histograms of phonon energy collection efficiencies of DMC samples each with 100 events, with no surface down-conversion setting. **Left:** 10 keV 0 V and 1 keV 50 V samples with no energy cut-off. **Right:** 10 keV 0 V and 1 keV 50 V samples where phonons with energy below 340×10^6 eV were eliminated.

6.2 Verification of Default G4CMP Configuration

As a preliminary test, we generated (for both 0 V and 50 V) one sample with a macro file that does not include the surface anharmonic down-conversion command and another with the surface anharmonic down-conversion command where all coefficients are set to 0. A comparison of the resulting phonon collection efficiencies reveals that the default G4CMP configuration indeed only models down-conversion in bulk. The color maps in Figure 5 also inform that events at the radial edges of the detector have lower than average energy collection efficiencies.

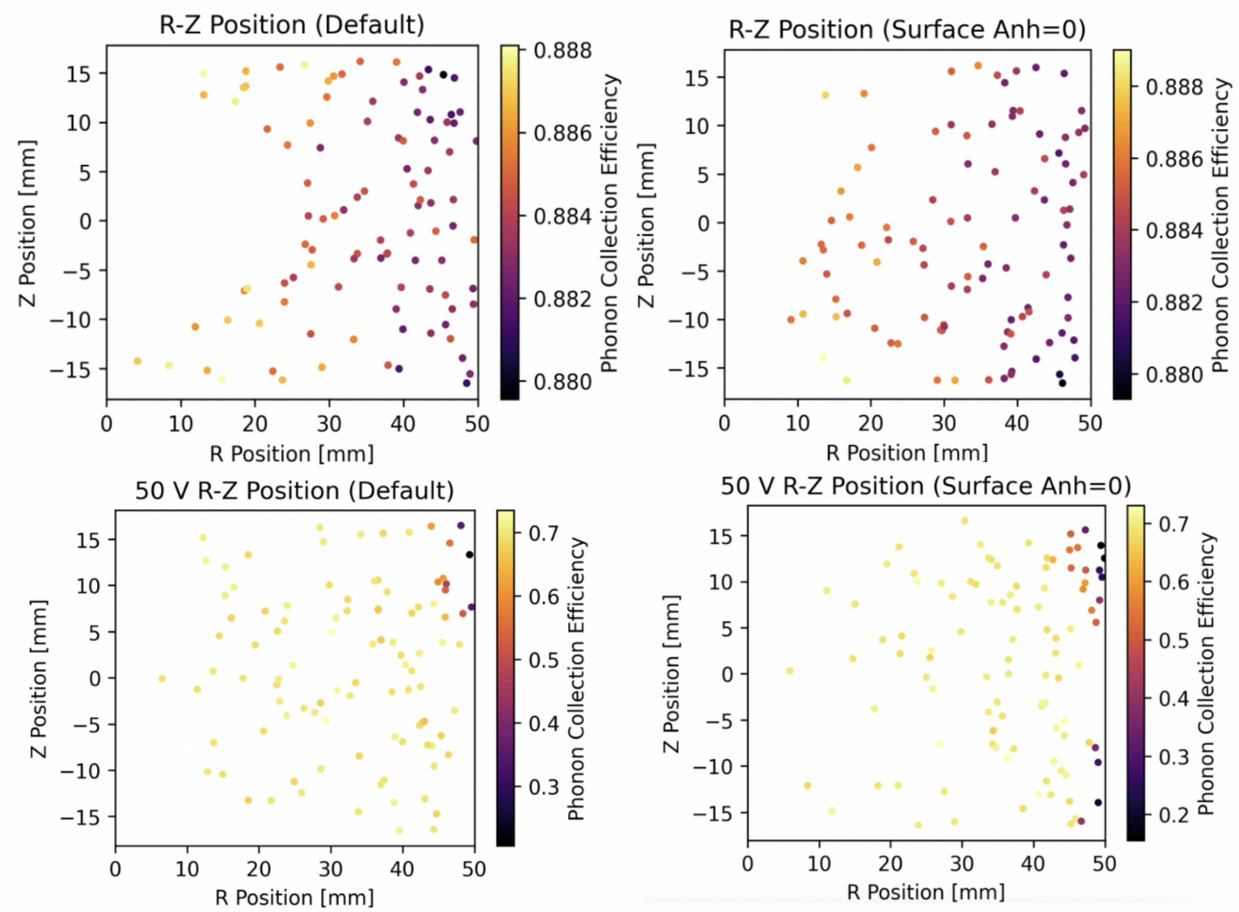

Figure 5: Z Position vs R position plots of energy depositions of DMC samples each with 100 events. The colors represent the phonon energy collection efficiencies. **Left:** 10 keV 0 V and 1 keV 50 V samples with no surface anharmonic down-conversion setting. **Right:** 10 keV 0 V and 1 keV 50 V samples with surface anharmonic down-conversion set to 0.

6.3 Effect of Simulating Down-conversion at Detector Sidewall

6.3.1 Phonon Energy Collection Efficiency

To investigate the effect of simulating surface anharmonic down-conversion, we set $c_5 = 1 \times 10^{-17}$ s for the 1 keV 50 V sample, which corresponds to an initial down-conversion rate of

$$\left(\frac{1000 \text{ eV}}{4.135 \cdot 10^{-15} \text{ eV s}}\right)^5 \cdot \left(10^{-17} \text{ s}\right)^4 \approx 8.3 \times 10^{18} \text{ Hz} \tag{8}$$

which is around 14 orders of magnitude lower than the bulk down-conversion rate given by

$$\left(\frac{1000 \text{ eV}}{4.135 \cdot 10^{-15} \text{ eV s}}\right)^5 \cdot \left(1.6456 \times 10^{-54} \text{ s}^4\right) \approx 1.4 \times 10^{33} \text{ Hz}. \tag{9}$$

We simulated anharmonic down-conversion only at the detector sidewalls, which account for most of the bare surfaces. From Figure 6, it is evident that phonon energy collection efficiencies decrease significantly when sidewall down-conversion is included. Specifically, the mean ϵ_{ph} decreased by approximately 45% compared to simulations where all surface down-conversion coefficients were set to zero. Furthermore, in the left plot, ϵ_{ph} values were mostly uniform, with a few outliers at radii (R positions) greater than 45 mm. In contrast, the right plot shows a gradual decrease in ϵ_{ph} as the radius increases, indicating a clear dependence of ϵ_{ph} on the radial position. This result aligns with the expectation that energy depositions closer to the detector radial edge were more likely to produce phonons that eventually collide with the sidewall and undergo down-conversion. Thus, more energy is lost in this process.

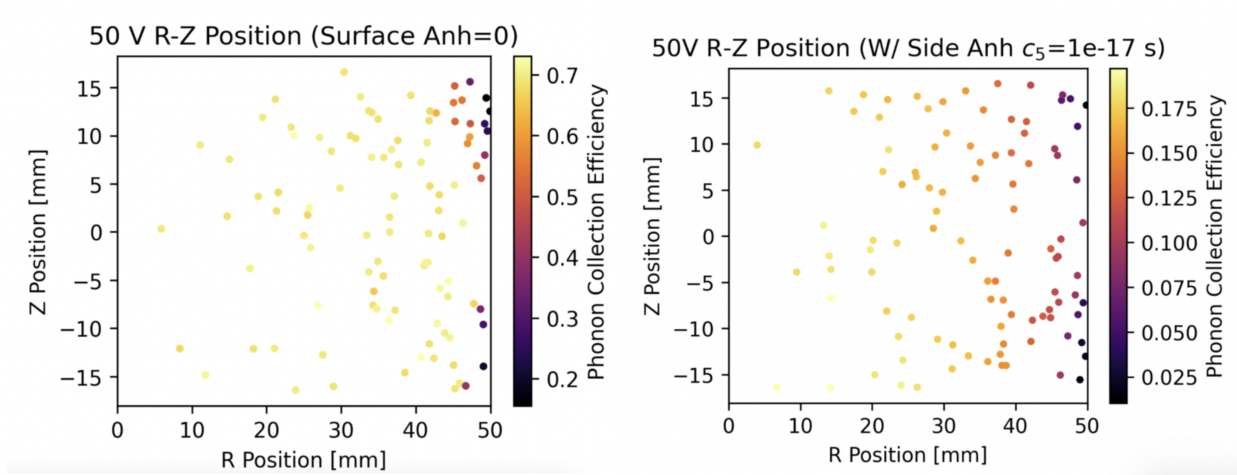

Figure 6: Z position vs R position plots of energy depositions of DMC samples each with 100 events. The colors represent the phonon energy collection efficiencies. **Left:** 1 keV 50 V sample with no surface anharmonic down-conversion. **Right:** 1 keV 50 V sample with c_5 set to 1×10^{-17}.

This comparison implies that simulating surface down-conversion that occurs at a much lower rate than bulk down-conversion effectively decreases the phonon collection efficiency.

6.3.2 Phonon Energy Distribution Among Channels

One of the key motivations for this study was the observed discrepancy in energy absorption by the outer ring channels between simulation and experimental data [1]. This discrepancy occurs in both the 0 V and 50 V cases but is more pronounced at 50 V. The difference between 0 V and 50 V can be attributed to the influence of the applied voltage on charge transport. At higher voltages, charge carriers predominantly travel in directions parallel or antiparallel to the electric field, whereas at 0 V, their motion follows a random walk. This behavior enhances the sensitivity of the radial position in the high-voltage case, making events near the detector's radial edges more likely to generate phonons collected by the outer ring channels.

Indeed, from Figure 7, the 50 V DMC sample recorded approximately 18% of the total energy in the A channels, compared to only 14% of the total phonon amplitude recorded in the A channels for the CUTE sample. Since phonon amplitudes are proportional to the collected energy, these percentages can be directly compared.

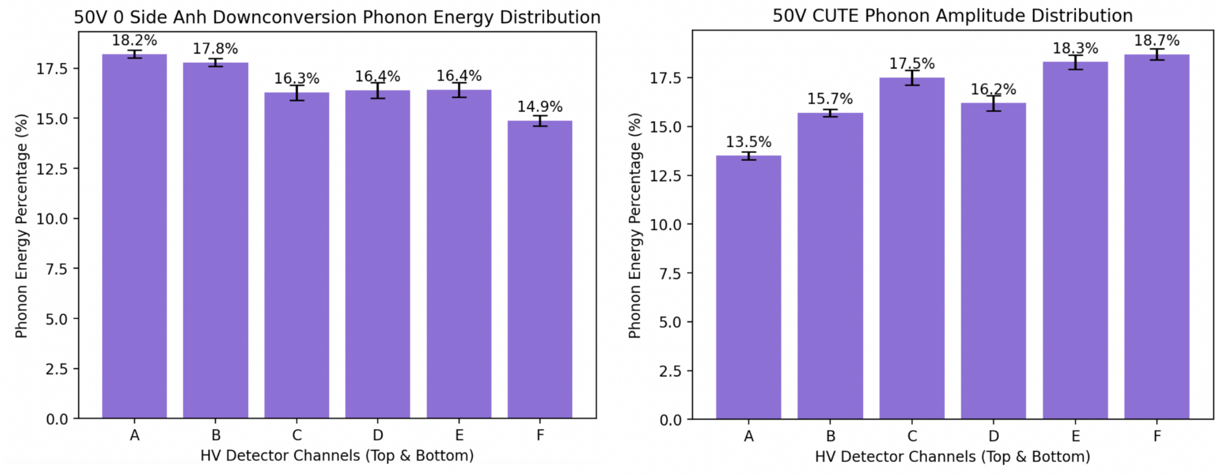

Figure 7: Bar plots of phonon energy/amplitude distributions among the six (top and bottom) channel pairs in HV detector. The error bars are given by the standard deviation of percentages for each event divided by the square root of the total number of events. **Left:** 1 keV 50 V DMC sample with no surface anharmonic down-conversion. **Right:** 1 keV 50 V CUTE data.

Since all channels were designed to have equal areas and WIMP particles should interact uniformly with the detector, we would initially assume that they record the same total energy. Moreover, since the DMC sample and CUTE data contains events randomly distributed within the detector, fluctuations within one to two percent is reasonable. However, due to edge effects in the electric field and defects at the crystal boundaries [1], we expect that even for events that occurred near the outer edge, the A and B channels would record less energy than the other channels would have if the event occurred near their regions. Thus, the outer ring channels are expected to record less total energy than the other channels. This theoretical understanding is verified by real data (see right plot of Figure 7).

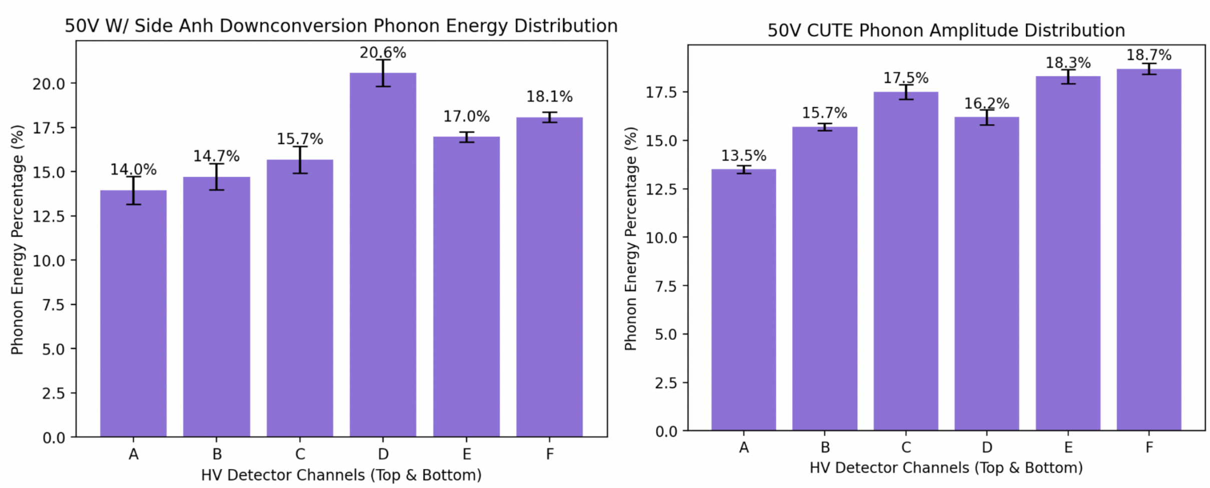

Figure 8: Bar plots of phonon energy/amplitude distributions among the six (top and bottom) channel pairs in HV detector. The error bars are given by the standard deviation of percentages for each event divided by the square root of the total number of events.**Left:** 1 keV 50 V DMC sample with c_5 set to 1×10^{-17} s for the detector sidewall. **Right:** 1 keV 50 V CUTE data.

When surface down-conversion is simulated at the sidewalls (again with $c_5 = 1 \times 10^{-17}$ s), the A and B channels record only around 14% and 15% of total energy, respectively. These values align closely with those of the CUTE data within one error bar. This shows that simulating surface down-conversion is a viable approach to resolve the discrepancy between simulation and experimental data.

7 Conclusion

In conclusion, anharmonic down-conversion is responsible for phonon energy loss within SuperCDMS detector crystals, making it an essential process to the detection of temperature changes due to particle interactions. Due to limited understanding of surface down-conversion, only bulk down-conversion is modeled by the default configuration of G4CMP. We generated DMC samples with surface down-conversion by setting the coefficient that scales the fifth power of phonon frequency. We compared the phonon energy collection efficiencies (ϵ_{ph}) of samples without phonon down-conversion and those of samples with down-conversion at detector sidewalls. The results show that setting a down-conversion rate of 8.3×10^{18} Hz reduces mean phonon energy collection efficiency by 45%, and the ϵ_{ph} spectrum clearly depends on the radial position of the event, where events near the radial edge have low collection efficiencies. Furthermore, this down-conversion rate resolves the discrepancy where the outer ring channels in DMC record above average proportion of total energy compared to real data measured at CUTE. Due to the consumption of time and memory, the surface down-conversion coefficients experimented in this study are limited in number. Running a 100-event sample with surface down-conversion on average takes around four hours.

For future studies, it is essential to explore the effects of a wider range of coefficients and determine the sensitivity of various features to these changes. Generating larger simulation samples would also be beneficial in achieving improved statistical accuracy. Additionally, it is important to acknowledge that while simulating surface down-conversion improves alignment between certain features and real data, it may not be the primary cause of the observed discrepancies. Several potential areas warrant further investigation, including the nature of phonon reflection at surfaces. More detailed studies could focus on examining the angles at which phonons reflect off surfaces and the energy distributions resulting from phonon down-conversion events.

References

[1] Cui, S. (2024). Comparison of Channel Pair and Correlation Features Between CUTE and DMC Data.

[2] Cui, S. (2024). Optimizing Machine Learning Techniques for Dark Matter Detection: Enhancing Position Resolution in SuperCDMS Detectors.

[3] Kelsey, M. H. (2023). G4CMP: Condensed Matter Physics Simulation Using the Geant4 Toolkit. Nuclear Instruments and Methods A. Retrieved from https://arxiv.org/abs/2302.05998

[4] Cormier R. & and Hui M. (2019). Modelling Surface Anharmonic Phonon Downconversion in SuperCDMS Simulations. *Slac. Conflu.*

[5] Perry, W. (2024). Statistical Modeling of Carrier Transport and Scattering in Cryogenic Dark Matter Detectors.

[6] Pyle, M. (2012). Optimizing the Design and Analysis of Cryogenic Semiconductor Dark Matter Detectors for Maximum Sensitivity. [PhD Thesis, Stanford University]. Retrieved from https://www.slac.stanford.edu/exp/cdms/ScienceResults/Theses/mpyle.pdf

[7] Philip J. & Breazeale M. A. (1983). Third-order elastic constants and Grüneisen parameters of silicon and germanium between 3 and 300° K, Journal of Applied Physics, *54*(2).

[8] Tamura, S. (1984). Spontaneous decay rates of LA phonons in quasi-isotropic solids. *Physical Review B*, *31*(4).

[9] Michaud, E. (2024). G4CMP Configuration File. Retrieved from https://github.com/kelseymh/G4CMP/blob/master/CrystalMaps/Ge/config.txt

[10] Reyes, A. Z. (2024). Collection Efficiency study. *Slac. Conflu.*

[11] Perry, W. (2024). Statistical Modeling of Carrier Transport and Phonon Emission.